2009 American Control Conference
Hyatt Regency Riverfront, St. Louis, MO, USA
June 10-12, 2009

Adaptive Control in the Presence of Quantization and Saturation: Application to Laser Beam Steering by a Liquid Crystal Device

Pawel K. Orzechowski, Steve Gibson and Tsu-Chin Tsao
Mechanical and Aerospace Engineering
University of California, Los Angeles 90095-1597

Dan Herrick and Victor Beazel
Optics Division, AFRL/DES, Directed Energy Directorate
U.S. Air Force Research Laboratory, Kirtland AFB, NM 87117-5776

Milind Mahajan, Bing Wen and Bruce Winker
Teledyne Scientific Company
1049 Camino Dos Rios, Thousand Oaks, CA 91360

Abstract— **This paper presents an investigation of adaptive control for a system with control quantization and magnitude and rate saturations. The application is laser beam steering by a liquid crystal device. The effects of using a linear time-invariant feedback loop along with the adaptive controller are discussed, as well as the effects of using nonlinear and linear plant models in the adaptive controller. In contrast to conventional fast steering mirrors, the liquid crystal device optically redirects the laser beam and has no moving parts or structural resonance, which often requires a stabilizing feedback controller prior to the adaptive controller. Simulation and experimental results demonstrate the effects on the adaptive control performance of choices of linear or nonlinear, and open or closed-loop plant models, and show which choices yield best performance.**

Index Terms: Control of lasers, optical jitter, adaptive control, liquid crystal beam steering device

I. Introduction

Quantization and saturation inevitably exist in digitally controlled systems which otherwise present linear time invariant dynamics. Both amplitude and rate saturation of the control input occur commonly in electromechanical systems. In most cases, the effects of quantization and saturation are negligible for control design and analysis; the systems usually are designed to operate within saturation constraints, the quantization levels often are small for digital and analog interfaces, and the limited bandwidth of system dynamics often smooths quantization jitter at the output.

Quantization and both magnitude and rate saturation are not negligible in the recently developed liquid crystal devices used for laser beam steering [1]–[3]. Because liquid crystal devices have no moving parts and require low operating power, they are a potentially attractive alternative to fast steering mirrors for control actuators in laser beam stabilization. However, the physics and design of the liquid crystal devices for beam steering impose substantial quantization levels and limited range of angles and rates.

The combined effects of quantization and saturation for the liquid crystal device in the adaptive control system were first considered in [2], [3], which demonstrated the importance of placing the nonlinearities explicitly in the plant model to render stable response. This paper further investigates the effect of quantization and saturation on adaptive beam control with and liquid crystal device by comparing the performance of the adaptive controller in two implementations: In one case, the adaptive control loop augments a linear time-invariant (LTI) feedback control loop; in the other case, there is no LTI loop. Previous papers on adaptive beam control, including [1], [2], have used an inner LTI feedback loop to reject low-frequency errors and stabilize lightly damped fast-steering mirror modes when necessary. Since the liquid crystal device is open-loop stable, the LTI loop is not necessary, and the results here show that because of the quantization and saturation the LTI loop degrades the performance of the adaptive loop, though not severely.

Laser beam steering plays a central role in contemporary technological applications such as free-space optical communications, high-energy laser (HEL) systems, scanning optical lithography and laser welding and cutting. Such applications demand precise pointing in the presence of disturbances that often have multiple bandwidths. Recently developed adaptive control methods can track and reject non-stationary, high-bandwidth jitter in laser beams. The adaptive filtering methods used in these controllers include least-mean-square (LMS) adaptive filtering [4]–[8] and recursive least-squares (RLS) adaptive filtering [9]–[15]. In [4]–[15], fast steering mirrors were used to steer the laser beams.

The paper is organized as follows. Section II describes the laser beam jitter control experiment using the liquid crystal

This work was supported by U.S Naval Office of Research under Grant N00014 07-1-1063.

Pawel K. Orzechowski is currently with Northrop Grumman Aerospace Systems, Controls System Department, Redondo Beach, CA.

978-1-4244-4524-0/09/$25.00 ©2009 AACC

device as beam steering actuator. Section III presents the nonlinear system model, which includes quantization as well as amplitude and rate saturation, with and without a linear stabilizing feedback loop. Section IV describes the adaptive control system. Section V presents the simulation results, Section VI presents experimental results and analysis, and Section VII contains the conclusions.

II. Experimental System Description

The transmissive liquid crystal beam steering device was developed by Teledyne Scientific Company (TSC) of Thousand Oaks, CA. The device uses dual frequency liquid crystal optical phased array (OPA) technology [16], [17] to produce a compact, low-power, high-speed beam-steering device for electro-optic systems. As opposed to other optical phased arrays, the Teledyne device has no phase resets across the aperture. The device, which has no movig parts, employs dual frequency liquid crystals in the near infrared because this class of materials surpasses all others in terms of switching speed, phase stability and electronic controller size, weight and power. The device has a 2 cm aperture, a ± 300 μrad field of regard in both directions, 2 μrad steering resolution, 3.125 kHz frame rate and 24 mrad/sec slew rate.

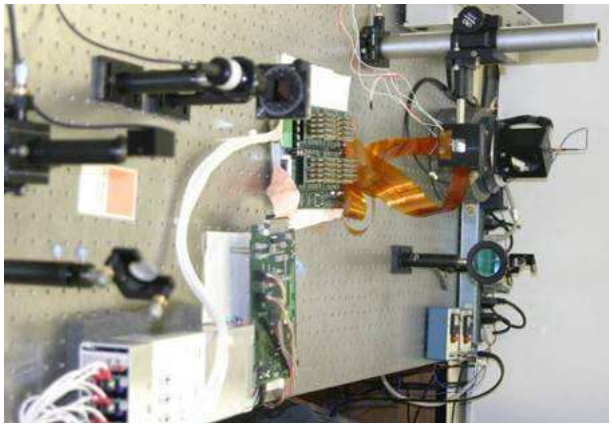

Fig. 1. Laser beam steering experiment with liquid crystal device.

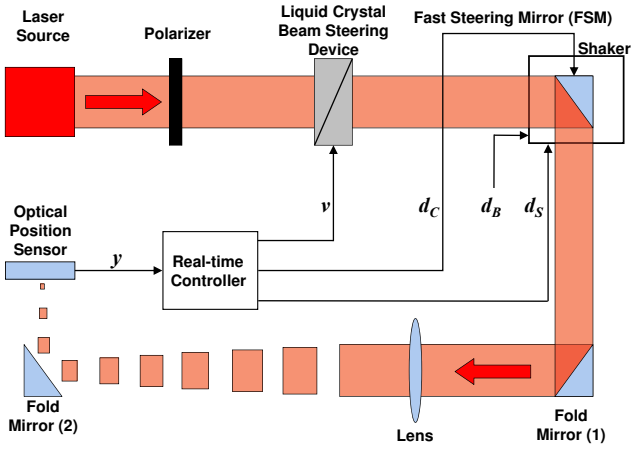

Fig. 2. Diagram of the experiment.

The physics and design of the liquid crystal device and Teledyne's device controller are discussed in [1], [2].

The device controller allows high-level control of the beam-steering device by a system level controller (xPC Target in this paper). The device controller accepts 8-bit digital control signals that command the controller to increase or decrease the beam deflection along X and Y directions by angles up to 8 μrad, in increments of 2 μrad. The device controller returns a digital timing output to synchronize the system controller with the device controller.

Figs. 1 and 2 show the beam steering experiment, which includes a 980nm laser, a wire grid linear polarizer, the liquid crystal beam steering device, a fast steering mirror (FSM) mounted on a shaker, a rigid folding mirror, a convergent lens, followed by a second rigid folding mirror and an optical position sensor (OPS).

MATLAB's xPC Target real-time software processes the control algorithms on a 3.6 GHz Pentium operating at the sample-and-hold rate of 3125 Hz, which is determined by the liquid crystal device's driver electronics. The inputs to the controller are the position of the laser spot on the plane of the sensor, denoted by the two-dimensional vector y, and the scalar measurement a_M from an accelerometer mounted on top of the case for the fast steering mirror. The output of the controller is the two-dimensional command vector v sent to the liquid crystal device.

There are three independent sources of jitter, denoted by d_B, d_C, d_S in Fig. 2. The shaker on which the fast steering mirror is mounted responds to building vibration denoted by d_B. The fast steering mirror and the shaker are driven by the commands d_C and d_S, respectively, which are generated in xPC Target but not given to the control loops.

III. System Models

The liquid crystal device is representative of systems with input quantization and amplitude and rate saturation. In Fig. 3, the part of the block diagram in solid lines represents the device hardware, including the Teledyne device controller. The part of Fig. 3 in dashed lines, which does not represent device hardware, will be explained later.

The input to the device controller is the two-dimensional rate command from the xPC Target, and the output of the liquid crystal device is the pair of beam angles. The three delays represented by the z^{-3} block are due to the electronics in the driver and the response time of the liquid crystal device. The loop with the z^{-1} block represents integration of the rate to yield displacement.

The device controller receives commands at the rate of 3125 Hz. These slew-rate commands are limited to integer values between -4 and +4; hence the rate limit and quantization blocks in Figure 3. The liquid crystal device can steer the beam to 301 discrete states in the range of ± 300 μrad, yielding 2 μrad in each incremental step. While the device's state transition occurs rapidly within each sample-and-hold interval (1/3125 sec), the quantization and saturation limits on angle and slew rate affect control system performance.

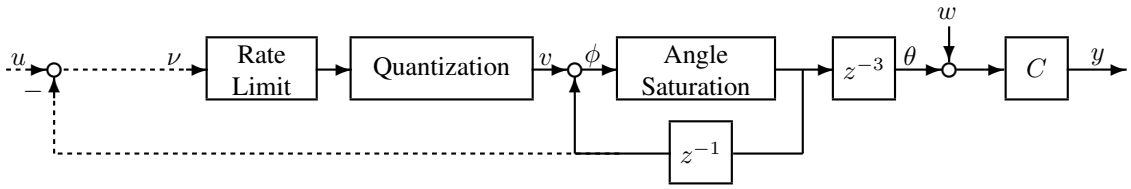

Fig. 3. Block diagram of the liquid crystal device. Solid lines represent hardware. The signals are two-dimensional.

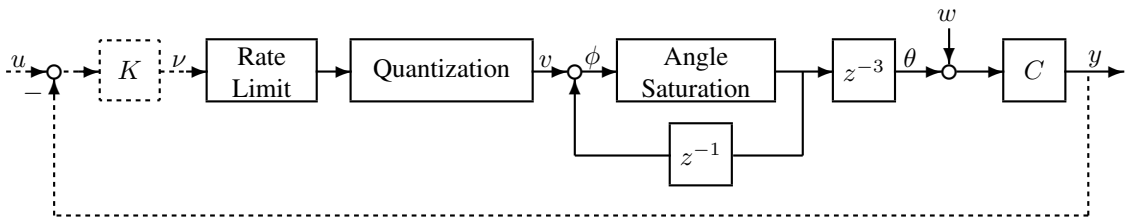

Fig. 4. Block diagram of the liquid crystal device with LTI feedback control loop.

The saturation blocks in Fig. 3 are characterized by the following for each axis ($i = 1, 2$):

$$\text{Rate Limit Output} = \begin{cases} \nu_i, & |\nu_i| \leq 4, \\ 4, & \nu_i > 4, \\ -4, & \nu_i < -4, \end{cases} \tag{1}$$

$$\text{Angle Saturation Output} = \begin{cases} \phi_i, & |\phi_i| \leq 150, \\ 150, & \phi_i > 150, \\ -150, & \phi_i < -150. \end{cases} \tag{2}$$

The quantization block in Fig. 3, rounds the input to the nearest integer value.

For the purpose of beam control, it is desirable to convert the device rate input to angle input because the measured output is displacement. Two methods for conversion are shown in Fig. 3 and Fig. 4, respectively. In Fig. 3, the dashed lines are added to the device hardware model to convert the plant input from rate to position command. The plant model in Fig. 3 is referred to as open-loop plant model, since the added dashed lines are not feedback actions. Fig. 4 shows a typical beam position feedback loop, which forms a new closed-loop plant with beam position as the command input.

The gain matrix C in Fig. 3 and Fig. 4 converts the beam angles θ to the position measurements y given by the optical position sensor (OPS). To determine C, the liquid crystal beam steering device was driven with an open-loop white-noise sequence ν (without the control loops closed). The resulting output sequences showed that, as expected, C is diagonal. A least-squares fit between the input and output data yielded $C = \text{diag}\begin{bmatrix} 0.0130 & 0.0185 \end{bmatrix}$.

The output disturbance w represents the combined effect of the jitter sources d_C and d_S and the building vibration d_B. As shown in Fig. 5, d_S and d_B drive the shaker, and d_C drives the disturbance fast steering mirror (FSM in Fig. 5). Any sensor noise associated with the optical position sensor would be added to the the signal y; however, careful measurements of the output of the OPS have shown that sensor noise is negligible in the experiments reported here.

The gain matrix in the LTI feedback loop is $K = \text{diag}\begin{bmatrix} 2 & 2 \end{bmatrix}$. This gain approximately maximizes the error-rejection bandwidth with minimal amplification of high-frequency disturbance. Attempting to increase the bandwidth by increasing K would produce greater amplification of high-frequency disturbance and sensor noise.

In subsequent discussion, the true plant is denoted by G, which is stable. The plant model $\hat{G}_{NL}$ is a stable nonlinear operator representing the nonlinear model of the true plant G. The linear plant model $\hat{G}_L$ neglects the quantization and saturation in G. These transfer functions can refer to either the open-loop plant in Fig. 3 or the closed-loop plant in Fig. 4. Of course, G, $\hat{G}_{NL}$ and $\hat{G}_L$ for Fig. 3 are different from those for Fig. 4. The linear plant models are

$$G_L = CKz^{-3} \quad \text{for Fig. 3,} \tag{3}$$

$$G_L = CK\left[z^3 - z^2 + CK\right]^{-1} \quad \text{for Fig. 4.} \tag{4}$$

IV. Adaptive Control Loop

Figure 6 shows the block diagram of the adaptive controller. This block diagram is the same whether the plant is the open-loop plant in Fig. 3 or the closed-loop plant in Fig. 4, but the the choices for $\hat{G}_a$ and $\hat{G}_c$ are different.

The signal $\hat{w}$ in Fig. 6 is an estimate of output disturbance, either open-loop or closed-loop, depending on whether the plant is that in Fig. 3 or that in Fig. 4. When the plant is that in Fig. 3, $\hat{w}$ estimates Cw where w is the disturbance in Figs. 3 and 4. When the plant is that in Fig. 4, $\hat{w}$ estimates the signal y that would be generated by the closed-loop plant in Fig. 4 with $u = 0$.

The plant model $\hat{G}_c$ in Fig. 6 can be either $\hat{G}_L$ or $\hat{G}_{NL}$. As shown in Fig. 6,

$$\hat{w} = y - \hat{G}_c u. \tag{5}$$

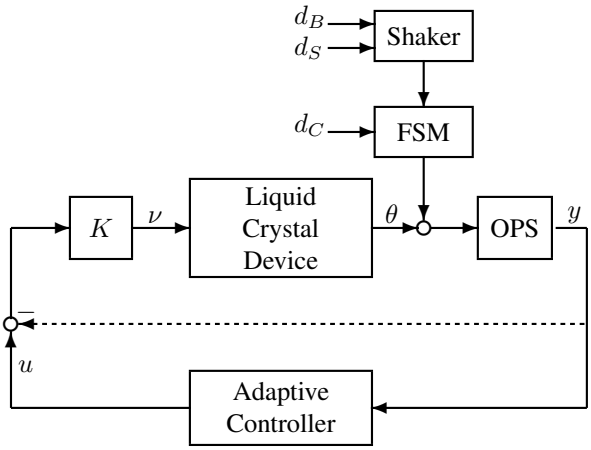

Fig. 5. Block diagram of the complete system. d_S = disturbance command to shaker; d_B = building vibration; d_C = disturbance command to FSM; d_M = response of FSM; θ = beam angle from liquid crystal beam steering device; y = beam position on sensor; u and ν = control commands. The dashed line indicates the LTI feedback control loop.

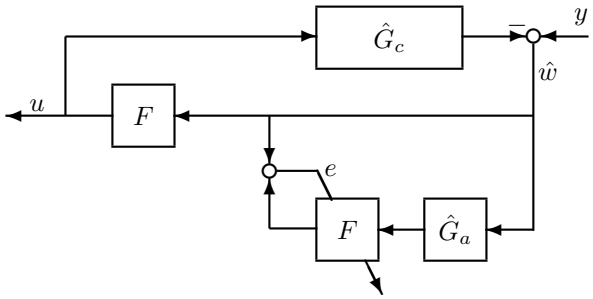

Fig. 6. Block diagram of the adaptive controller. $\hat{G}_c$ and $\hat{G}_a$ are estimates of G; F = adaptive FIR filter; $\hat{w}$ = estimate of the output disturbance; e = sequence to be minimized.

Taking $\hat{G}_c = \hat{G}_{NL}$ yields a more accurate $\hat{w}$ and better adaptive control performance.

For stability analysis, the adaptive control system can be considered as a feedback loop consisting of two blocks, the model error $G - \hat{G}_c$ and the adaptive FIR filter F. Since the nonlinear model is closer to the true plant than the linear model is, using $\hat{G}_c = \hat{G}_{NL}$ in the adaptive controller produces greater stability robustness.

The adaptive filter F implicitly tracks the statistics of the disturbance and identifies gains to minimize the RMS value of the prediction error e. The precise least-squares criterion minimized by the adaptive filter is the RMS value of the sequence e, as indicated by the slanted arrow in Fig. 6. Since the two channels of the plant are modeled as uncoupled for control design, the LTI and adaptive control loops for the two plant channels are uncoupled. In each channel then, the operator $\hat{G}_a$ can be selected as the linear plant model G_L or nonlinear model G_{NL}.

Figure 6 yields the following equations:

$$y = (1 + \hat{G}_c F)\hat{w}, \tag{6}$$

$$e = (1 + F\hat{G}_a)\hat{w}, \tag{7}$$

$$y = e + (\hat{G}_c F - F\hat{G}_a)\hat{w}. \tag{8}$$

In the ideal case where the true plant G is linear and known, $\hat{G}_c = \hat{G}_a = G$. Then, under stationary disturbance w, F converges to a linear time-invariant FIR filter that minimizes the variance of e in steady state. This F commutes with $G = \hat{G}_c = \hat{G}_a$ so that, according to (8), F also minimizes the variance of the steady-state output y [18].

Even for nonlinear G, $\hat{G}_a = \hat{G}_L$ is preferable to $\hat{G}_a = \hat{G}_{NL}$ for two reasons: If $\hat{G}_a$ is nonlinear it will not commute with F. Also, if $\hat{G}_a = \hat{G}_{NL}$, the signal $\hat{G}_a\hat{w}$, which is used in adaptively identifying F as shown in Fig. 6, will have more spectral content than $\hat{w}$ has, due to the nonlinear filter $\hat{G}_{NL}$. Thus the adaptive filter prediction error e and the output y, in view of (8), will be larger than those for the case $\hat{G}_a = \hat{G}_L$.

The main component of the adaptive controller is the recursive-least-squares (RLS) adaptive filter F in Fig. 6, but the adaptive filter is not the focus of this paper. The adaptive filter has finite impulse response (FIR) and order N. The adaptive filter has the lattice realization in [19]. The order-recursive structure of the lattice filter allows the adaptive controller to have variable order, generating adaptive control commands of all orders $n \leq N$. During adaptation, lattice-filter orders $n < N$ are used, with the order increasing to the maximum order N in steady-state. For the results in this paper, $N = 60$. The improved transient response provided by lattice-filter based variable-order adaptive control is discussed in detail in [13], [15].

V. Simulation Results

Simulations were performed for both the open-loop and closed-loop plant models (i.e., Fig. 3 and Fig. 4) and with the four possible combinations of the corresponding linear or nonlinear models for $\hat{G}_c$ and $\hat{G}_a$. Also, two types of disturbance were used. In one group of simulations, the disturbance was a sine wave with a constant bias, and in another group of simulations, an output disturbance recorded from an the experiment was used. Axis 2 had greater and more complex disturbance in the experiments, so simulation results are discussed for Axis 2 only.

In the first simulation, the disturbance w was a constant bias of 5.5 (11 μrad) and a sine wave of amplitude 5 at 200 Hz. This disturbance only triggers the quantization but not saturation nonlinearity. The simulations for 10th order adaptive FIR filter show that the adaptive controller with $\hat{G}_c = \hat{G}_{NL}$, $\hat{G}_a = \hat{G}_L$ and without the LTI feedback loop gives the best performance; i.e. smallest steady state RMS value of the output y. In this case, the steady state output signal before the optical gain C is always within one quantization step (± 0.5 μrad). The performance without LTI feedback control is better because the prediction error e converges to zero and the filter F converges for this case but not with LTI feedback control. Even with only a single frequency in the disturbance w, the feedback loop generates higher harmonics and almost periodic signals due to the nonlinear effects of quantization and saturation in the plant. Figure 7 shows the time series of the output with and without the LTI feedback loop. The output produced

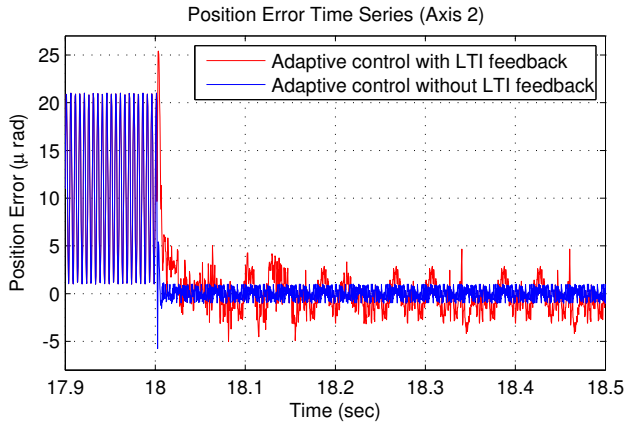

Fig. 7. Output time series from simulation with sinusoidal disturbance. Adaptive control begins at 18 sec.

by adaptive control with LTI feedback is substantially larger than that without LTI feedback, which is bounded within one quantization step.

In another simulation, the bias and/or amplitude of the sine wave was increased to also trigger the magnitude and/or rate saturation limit. As expected, $\hat{G}_c = \hat{G}_L$ always gave the worst performance or instability due to the inability to estimate the disturbance accurately, and the feedback loop modeling error discussed in the previous section.

For the final simulations, the disturbance was the open-loop disturbance from the experiments described in Section VI. This disturbance is the output measured by the position sensor when the liquid crystal device is not under any control action but the disturbances in the experiments are present. The results are shown in Fig. 8. The similarity between the power spectra in Fig. 8 and those in Fig. 9 from the experiments validate the plant models in Section III.

VI. Experimental Results

In the experiment, the adaptive controller using $\hat{G}_c = \hat{G}_{NL}$ and $\hat{G}_a = \hat{G}_L$ was used for the open-loop and closed-loop plant models (i.e., Fig. 3 and Fig. 4). The jitter commands d_C and d_S shown in Fig. 5 were produced by passing white noise sequences through band-pass filters in xPC Target. (As stated earlier, these command sequences were not given to the control loops.) Axis 1 and Axis 2 refer to the directions in which the laser spot was measured on the optical position sensor. Axis 1 is horizontal, and Axis 2 is vertical.

Fig. 9 shows the output errors for the experiment. For the results presented in this paper, the two channels of the output error y measured by the optical position sensor are converted to μrad. The jitter on Axis 1 has smaller amplitude and bandwidth than than on Axis 2 because the disturbances act mainly on Axis 2.

The time series of the output errors and the RMS values in Table I show that the adaptive control loop greatly reduces the output errors compared to both open loop and LTI feedback control. Most importantly, the effect of the LTI

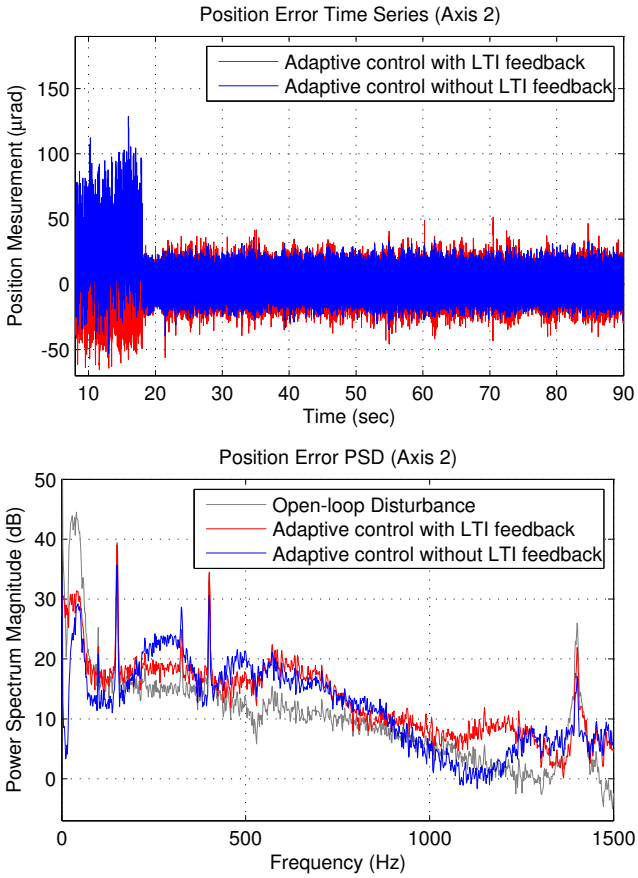

Fig. 8. Simulation results for experimental output disturbance (in gray).

feedback loop on the performance of the adaptive loop is similar to the effect in the simulations: The output error produced by the adaptive controller has significantly higher power in low frequencies when the LTI feedback loop is used than when it is not used.

TABLE I
Steady-state RMS output position errors (μrad)

Control Loops	Axis 1 Experiment	Axis 2 Experiment	Axis 2 Simulation
LTI Feedback Only	16.7	19.6	19.7
Adaptive + LTI Feedback	2.5	9.2	6.9
Adaptive only	2.4	8.6	6.1

VII. Conclusions

This paper investigates the performance of an adaptive controller for a plant with non-linearities due to quantization and amplitude and rate saturations. The liquid crystal beam steering device used in the experiments for the paper has no moving parts and therefore is open-loop stable. Consequently, a stabilizing LTI feedback loop is not needed if adaptive control is used. The main conclusion of the paper is that an LTI feedback loop used in conjunction with the adaptive controller exacerbates the plant nonlinearities and degrades the performance of the adaptive loop. This is shown by both experimental and simulation results.

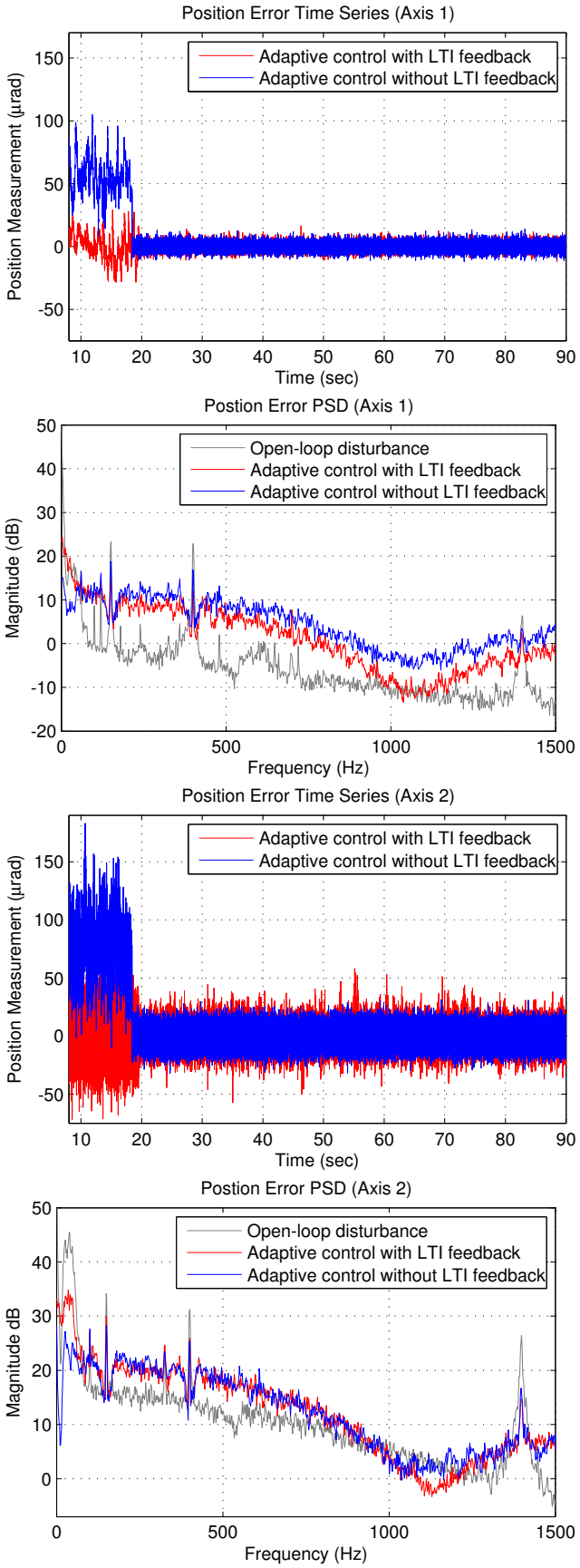

Fig. 9. Outputs y for experiments with and without the LTI feedback loop. Time series and PSDs are shown. Adaptive control begins at 19 sec. Top: Axis 1. Bottom: Axis 2; PSDs include the open-loop output disturbance.

A second conclusion of the paper pertains to two plant models used by the adaptive controller. For best performance, the adaptive controller should use a nonlinear plant model in estimating the output disturbance and a linear plant model in adaptively identifying an optimal feedforward filter.

References

[1] P. K. Orzechowski, J. S. Gibson, Tsu-Chin Tsao, Dan Herrick, Milind Mahajan, and Bing Wen, "Adaptive rejection of optical jitter with a new liquid crystal beam steering device," in *Defense and Security Symposium*. Orlando, FL: SPIE, April 2007.

[2] P. K. Orzechowski, Steve Gibson, Tsu-Chin Tsao, Dan Herrick, Victor Beazel, Milind Mahajan, Bing Wen, and Bruce Winker, "Nonlinear adaptive control of optical jitter with a new liquid crystal beam steering device," in *American Control Conference*. Seattle, WA: IEEE, June 2008.

[3] P. K. Orzechowski, "High-performance adaptive control of optical jitter in laser beam systems," Ph.D. dissertation, University of California, Los Angeles, Los Angeles, CA, 2007.

[4] Roger M. Glaese, Eric H. Anderson, and Paul C. Janzen, "Active suppression of acoustically induced jitter for the airborne laser," in *Proc. SPIE, Laser Weapons Technology*, vol. 4034. SPIE, July 2000, pp. 151–164.

[5] Mark A. McEver, Daniel G. Cole, and Robert L. Clark, "Adaptive feedback control of optical jitter using Q-parameterization," *Optical Engineering*, vol. 43, no. 4, pp. 904–910, April 2004.

[6] L. P. Fowler and R. Blankinship, "Experimental adaptive filtering and disturbance feedforward approach for flexible beam train control with single disturbance path," in *2006 Directed Energy Systems Symposium: Beam Control Conference*. DEPS, March 2006.

[7] Victor A. Skormin, Mark A. Tascillo, and Timothy E. Busch, "Adaptive jitter rejection technique applicable to airborne laser communication systems," *Optical Engineering*, no. 5, pp. 1263–1268.

[8] R. Joseph Watkins, Brij N. Agrawal, Young S. Shin, and Hong-Jen Chen, "Jitter control of space and airborne laser beams," in *International Communications Satellite Systems Conference & Exhibit*. Monterey, CA: AIAA, May 2004.

[9] B.-S. Kim, S. Gibson, and T.-C. Tsao, "Adaptive control of a tilt mirror for laser beam steering," in *Proc. of the American Control Conference*, Boston, MA, June 2004, pp. 3417–3421.

[10] Néstor O. Pérez Arancibia, J. S. Gibson, and Tsu-Chin Tsao, "Adaptive control of MEMS mirrors for beam steering," in *IMECE2004*. Anaheim, CA: ASME, November 2004.

[11] Néstor O. Pérez Arancibia, Neil Chen, J. S. Gibson, and Tsu-Chin Tsao, "Adaptive control of a MEMS steering mirror for suppression of laser beam jitter," in *American Control Conference*. Portland, OR: IEEE, June 2005.

[12] ——, "Adaptive control of a MEMS steering mirror for free-space laser communications," in *Optics and Photonics 2005*. San Diego, CA: SPIE, August 2005.

[13] N. O. Pérez Arancibia, N. Chen, S. Gibson, and T.-C. Tsao, "Variable-order adaptive control of a microelectromechanical steering mirror for suppression of laser beam jitter," *Optical Engineering*, vol. 45, no. 10, pp. 104 206–1–12, October 2006.

[14] P. K. Orzechowski, J. S. Gibson, and Tsu-Chin Tsao, "Adaptive control of jitter in a laser beam pointing system," in *American Control Conference*. Minneapolis, MN: IEEE, June 2006.

[15] ——, "Optimal suppression of laser beam jitter by high-order RLS adaptive control," *IEEE Transactions on Control Systems Technology*, vol. 16, no. 2, pp. 225–267, March 2008.

[16] Dong-Feng Gu, Bruce Winker, Donald Taber, Jeff Cheung, Yiwei Lu, Paul Kobrin, and Zhiming Zhuang, "Dual frequency liquid crystal devices for infrared electro-optical applications," vol. 4799. SPIE, 2002, pp. 37–47.

[17] Yu-Hua Lin, Milind Mahajan, Donald Taber, Bing Wen, and Bruce Winker, "Compact 4 cm aperture transmissive liquid crystal optical phased array for free-space optical communications," vol. 5892. SPIE, August 2005, pp. 58 920C1–10.

[18] B. Widrow and E. Walach, *Adaptive Inverse Control*. Englewood Cliffs, NJ: Prentice Hall, 1996.

[19] S.-B. Jiang and J. S. Gibson, "An unwindowed multichannel lattice filter with orthogonal channels," *IEEE Transactions on Signal Processing*, vol. 43, no. 12, pp. 2831–2842, December 1995.